Part I

Multiscale Simulation Theory

Atomistic and multiscale simulation research is one of the current focuses of computational mechanics. In Part One we present a group of recent research studies in this active research area. Some of the chapters presented in this book contain research topics that are reported or released for the first time in the literature, and they touch almost every aspect of multiscale simulation research. In Chapter 1, Wagner presents an atomistic-based multiscale method to simulate heat transfer and energy conversion, which is a recent development of the bridging-scale method. In Chapter 2, Tang presents a detailed account on how to provide an accurate boundary treatment for concurrent multiscale simulation including the bridging-scale method. In Chapter 3, Liu and Li present for the first time a novel multiscale method called multiscale crystal-defect dynamics (MCDD), which is intended for simulation of dislocation motion, nanoscale plasticity, and small-scale fractures. In Chapter 4, Fu and To discuss their ingenious construction of a novel nonequilibrium molecular dynamics, and then Park and Devel, in Chapter 5, apply a coarse-grained multiscale method to study electromechanical coupling in surface-dominated nanostructures. In this part, Wagner, Tang, and Park were the main members of Wing Liu's research group in the early 2000s and have worked with Wing Liu in developing the bridging-scale method. The last chapter of this part is contributed by Dr. Fish, who presents a multiscale design theory and design procedure for general composite materials based on a multiscale asymptotic homogenization theory.

1

Atomistic-to-Continuum Coupling Methods for Heat Transfer in Solids

Gregory J. Wagner
Sandia National Laboratories, USA

1.1 Introduction

New scientific and technical knowledge and advances in fabrication techniques have led to a revolution in the development of nanoscale devices and nanostructured materials. At the same time, improved computational resources and tools have allowed a continuously increased role for computational simulation in the engineering design process, for products at all scales. For many nano-mechanical or nano-electronic devices, models are sought that can accurately predict thermal and thermo-mechanical behavior under the range of conditions to which the devices will be subjected. However, at these small scales the limitations of continuum thermo-mechanical modeling techniques become apparent, as the effects of surfaces, grain boundaries, defects, and other deviations from a perfect continuum become important. Fourier's law, $\mathbf{q} = -\kappa \nabla T$ (where $\mathbf{q}$ is heat flux density, κ is the thermal conductivity, and ∇T is the local temperature gradient) may not be applicable, nor may macroscale stress and strain laws; in fact, concepts like stress, strain, and even temperature may be difficult to define at the atomic scale.

Atomistic simulation techniques like molecular dynamics (MD) provide a way to simulate these small-scale behaviors, especially when combined with an accurate and efficient interatomic potential or force law that allows simulations of billions of atoms. However, even the very largest MD simulations may not be able to capture large enough length scales to simulate the interscale interactions important in real devices (since, typically, a nanoscale device must at some level be addressable from the macroscale in order to provide useful function). Classical MD has other shortcomings, as well, especially for real geometries at finite temperatures. For example, a number of approaches are available for holding an MD simulation at fixed, constant temperature [1, 2]; however, it is more difficult to regulate a spatially varying temperature, except through the use of discontinuous "blocks" of atoms held at different temperatures.

Multiscale Simulations and Mechanics of Biological Materials, First Edition. Edited by Shaofan Li and Dong Qian.

Limitations of MD have led to the development of atomistic-to-continuum coupling methods [3, 4], in which a continuum description (usually a finite-element discretization) of the material is used where valid, but a discrete atomistic representation of the material is used in regions where the continuum assumptions break down. Such a breakdown may occur near defects like cracks or dislocations, or in domains where the feature size is not much larger than the interatomic spacing. The atomistic and continuum descriptions are coupled together at an interface or overlap region, usually by combining the Hamiltonians of the two systems [5] or by ensuring that internal forces are properly balanced [6]. The resulting system couples the momentum equations (or, for statics, the force equilibria) of the two regions. Formation of a seamless coupling is nontrivial even for the static case (see Miller and Tadmoor [7] for an excellent review). For the dynamic case, an additional difficulty is the wave impedance mismatch at the MD–continuum boundary, leading to internal reflection of fine-scale waves back into the MD domain. Several approaches have been studied for removing these unwanted wave reflections, usually through some form of dissipation; typically, the goal in these situations is to completely remove the outgoing energy and minimize the reflected energy, optimally to zero [8–10].

Often in these coupled simulations, even for dynamics, the system is assumed to be initially quiescent, with no thermal vibrations about the mean atomic positions. This assumption is the basis of energy dissipation techniques that seek to completely remove internal wave reflections by zeroing the incoming energy. However, a more realistic environment for an actual nanoscale device, or nanostructured material, is finite nonzero temperature. At finite temperatures, atoms can be assumed to be vibrating about their mean positions with some thermal energy, and lattice waves can be recognized as energy-carrying phonons. Of course, additional thermal energy may be added to the system in a number of ways, and may propagate outward through the MD–continuum interface. However, in this case the goal is not to dissipate away all incoming energy; rather, the correct balance of incoming and outgoing phonons should be maintained, at least in some averaged sense.

Recently, methods have been developed that couple MD and continuum simulations, while allowing two-way coupling of thermal information. These methods are the subject of this chapter. Two-way coupling implies that heat in the simulation can be transferred both in the fine-to-coarse scale direction (MD to continuum), and in the coarse-to-fine direction. In the former case, this means that energy added to the MD domain as thermal vibrations may be transported to the neighboring continuum and lead to an increased internal energy. Phenomena that may lead to an increase in thermal vibrations in the MD region include friction, laser heating, fracture, and plastic failure. In the coarse-to-fine direction, it is required that internal energy in the continuum can be transported into the MD domain and lead to increased vibrational energy.

In addition to the spatial partitioning into MD and continuum regions used in these methods, another important type of MD-to-continuum coupling for thermal fields is required for the simulation of heat transfer in metals. For insulators, heat transfer is dominated by phonons, energy-carrying vibrations in the atomic lattice. For metals and some semiconductors, however, a large amount of the thermal energy is transported by electrons; in classical MD simulations, this contribution of the electron field to heat transfer is missing, and thermal conductivity cannot be accurately predicted for these materials. On the other hand, the contributions of the atomic lattice to thermal behavior cannot be ignored, especially since many of the same phenomena discussed above (like friction) add heat to the system initially through lattice vibrational degrees of freedom. To address this, several authors have developed coupled atomistic-to-continuum implementations of the so-called two-temperature model (TTM) in which the thermal energy is partitioned between lattice vibrations and electrons [11, 12]; lattice motion is simulated using MD, while the electron temperature is solved using a continuum heat equation. Jones *et al.* [13] built on this previous work, using energy-conserving techniques similar to those used in partitioned domain coupling methods.

The central idea in much of this work is the simultaneous definition of a solution field, in this case temperature, at multiple scales. This idea stems from the multiscale work by Wing Kam Liu and his research group at Northwestern University. In the context of atomistic-to-continuum coupling, these ideas are captured in the bridging-scale method developed in that group [9, 14, 15], with earlier roots in the multi-resolution and bridging-scale approaches developed for continuum simulations [16–18].

In the remainder of this chapter we will summarize these newly developed methods, including the development of the theory behind them, along with some demonstrations and applications.

1.2 The Coupled Temperature Field

An important step in developing a coupled method is to clearly define the relationship between the atomic motions and the macroscale temperature. From classical (i.e., non-quantum) statistical physics, for a system of atoms at equilibrium, the system temperature T can be written in terms of the system kinetic energy [19]:

$$\frac{3}{2} n_{\mathrm{a}} k_{\mathrm{B}} T = \left\langle \sum_{\alpha} \frac{1}{2} m_{\alpha} |\mathbf{v}_{\alpha}|^2 \right\rangle, \tag{1.1}$$

where k_{B} is Boltzmann's constant, n_{a} is the number of atoms in the system, m_{α} and $\mathbf{v}_{\alpha}$ are the mass and velocity of atom α, and the angle brackets represent an ensemble or time average. Here, for simplicity, we are assuming that the mean velocity of each atom is zero, but more generally the velocity used in the temperature definition can be some perturbation about the mean (although the precise definition of the "mean" must be determined). From Equation (1.1), we can identify an atomic temperature T_{α}:

$$T_{\alpha} \equiv \frac{1}{3k_{\mathrm{B}}} m_{\alpha} |\mathbf{v}_{\alpha}|^2. \tag{1.2}$$

If it is assumed that the ensemble average in (1.1) is equivalent to an average over all atoms in an equilibrium system, then the system temperature at equilibrium is just an average of the atomic temperature T_{α} over the atoms.

In this work, we are primarily interested in nonequilibrium systems, where the temperature is not necessarily constant for the entire system, so that (1.1) does not apply directly. However, we can use the atomic temperature T_{α}, together with appropriate spatial- and time-averaging operators, to define a spatially varying macroscale temperature field in terms of the atomic temperature.

1.2.1 Spatial Reduction

First, we will assume that the spatially varying macroscale temperature can be represented by an interpolated field on a finite-element mesh (FEM), with an element size that is large compared with the interatomic spacing. This interpolation can be written as

$$T^{\mathrm{FE}}(\mathbf{X}, t) \equiv \sum_{I} N_I(\mathbf{X}) \theta_I(t). \tag{1.3}$$

In this expression, the sum is over the set of all nodes in the domain, θ_I is a temperature degree of freedom defined on node I, and $N_I(\mathbf{X})$ is the finite-element shape function associated with node I evaluated at $\mathbf{X}$.

One way to relate the macroscale and atomic temperature fields is to use a least-squares projection to minimize the difference between the interpolated temperature $T^{\mathrm{FE}}(\mathbf{X}, t)$ and the atomic temperature at every atomic location $\mathbf{X}_\alpha$. This is attractive, but leads to a matrix equation that must be solved. To simplify this projection, we approximate the projection matrix with a row-sum lumping to get a diagonal matrix (see Wagner *et al.* [20] for details), leading to a simple relationship between the nodal temperatures θ_I and the atomic temperatures, through a scaled shape function $\hat{N}_I$:

$$\begin{aligned} \theta_I &= \sum_{\alpha \in \mathcal{A}} \hat{N}_{I\alpha} T_\alpha, \\ \hat{N}_{I\alpha} &\equiv \frac{N_{I\alpha} \Delta V_\alpha}{\sum_{\beta \in \mathcal{A}} N_{I\beta} \Delta V_\beta}, \end{aligned} \tag{1.4}$$

where ΔV_α is the volume associated with atom α and $N_{I\alpha}$ is a shorthand notation for $N_I(\mathbf{X}_\alpha)$.

1.2.2 Time Averaging

Equation (1.4) defines an efficient spatial reduction from the atoms to the finite-element nodes. However, even when the number of atoms is much larger than the number of nodes, experience shows that the resulting nodal temperatures fluctuate in time even for what should be statistically steady states. To help reduce these fluctuations, we can define a time filtering operation as

$$\langle f(t) \rangle_\tau \equiv \int_{-\infty}^{t} f(t') G(t - t')\, \mathrm{d}t', \tag{1.5}$$

where $G(t)$ is a kernel function of the form

$$G(t) = \frac{1}{\tau}\, \mathrm{e}^{-t/\tau} \tag{1.6}$$

and τ is the time scale of our filtering operation. This filtering operation commutes with time differentiation, and for this choice of the kernel function $G(t)$ the time derivative of a filtered function can be rewritten as a simple, first-order ordinary differential equation:

$$\frac{\mathrm{d}}{\mathrm{d}t} \langle f \rangle_\tau = \frac{f - \langle f \rangle_\tau}{\tau}. \tag{1.7}$$

The usefulness of this property should be apparent: by using (1.7) to update time-filtered values, the filtered value of any quantity f can be computed without storing the time history of that quantity.

Ideally, the filtering timescale τ is much longer than the vibrational timescale of the atoms, but much shorter than the timescale associated with the expected macroscale temperature changes due to phonon heat transfer. If such a separation of scales is not possible, then a local macroscale temperature may be hard to define, and the only way to reduce fluctuations in the nodal temperatures may be to increase the number of atoms per node by coarsening the FEM.

By combining the spatial reduction (1.4) with the time filtering operator, we obtain a final expression relating the atomic motion to the finite-element temperature field:

$$\theta_I = \left\langle \sum_{\alpha \in \mathcal{A}} \hat{N}_{I\alpha} T_\alpha \right\rangle_\tau. \tag{1.8}$$

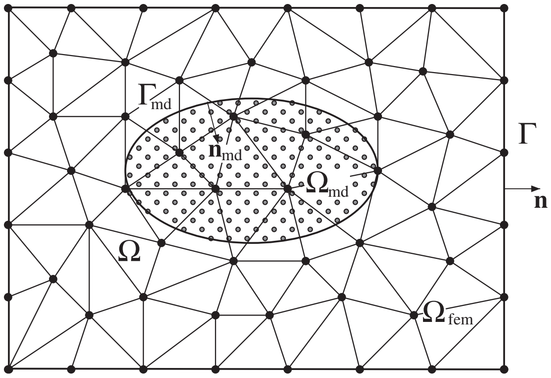

Figure 1.1 Coupled domain geometry

1.3 Coupling the MD and Continuum Energy

1.3.1 The Coupled System

The goal of our coupling strategy is to simulate domains decomposed as in Figure 1.1, in which a domain Ω is discretized with a FEM, while an internal portion of the domain Ω_{md} is represented by a set of atoms $\mathcal{A}$. The remaining portion of the domain in which there are no atoms but only finite elements is denoted Ω_{fem}; the boundary between the two subdomains is given by Γ_{md}, with normal vector $\mathbf{n}_{\text{md}}$ oriented into the MD region. The purpose of this partitioning is to use classical MD, with atomic forces derived from an interatomic potential, in those regions where the heat flow and corresponding dynamics are too complex to be described by a simple continuum heat transfer law (like the Fourier law). Thus, Ω_{md} will typically include defects, dislocation, grain boundaries, or any other nanoscale structures that may affect heat transfer.

To derive a coupled set of MD–FEM equations for this system, we assume that we can partition the total energy of the system into two parts that correspond to the two subdomains:

$$E^{\text{tot}} = E^{\text{md}} + E^{\text{fem}}. \tag{1.9}$$

For simplicity, we will assume that strain energy and the mean velocity of the FEM region can be neglected, so that the energy of the finite-element region is just the thermal energy $\rho c_p T^h$ integrated over Ω_{fem}:

$$E^{\text{fem}} = \int_{\Omega_{\text{fem}}} \rho c_p T^h(\mathbf{X}, t)\,\mathrm{d}V, \tag{1.10}$$

where the density ρ and the specific heat c_p are intrinsic properties that can both be related to the properties of the atomic lattice [19]. The energy of the MD region is the sum of the potential and kinetic energies of the atoms, with time filtering applied:

$$E^{\text{md}} = \left\langle U^{\text{md}} + \frac{1}{2}\sum_{\alpha} m_\alpha |\mathbf{v}_\alpha|^2 \right\rangle_\tau, \tag{1.11}$$

where U^{md} is the potential energy of the atoms in the MD region.

1.3.2 Continuum Heat Transfer

Outside of the MD region, in Ω_{fem}, we can write an equation for the evolution of the continuum temperature field:

$$\rho c_p \dot{T}(\mathbf{X}, t) = -\nabla \cdot \mathbf{q}(\mathbf{X}, t), \tag{1.12}$$

where $\mathbf{q}(\mathbf{X}, t)$ is the heat flux. We will assume that the continuum region is well described by the Fourier heat law with some known thermal conductivity κ:

$$\mathbf{q}(\mathbf{X}, t) = -\kappa \nabla T. \tag{1.13}$$

The thermal conductivity should be matched as well as possible to the value predicted by the MD system for a large, defect-free lattice; this can be calculated with a separate computation if needed.

The continuum heat equation applies only in Ω_{fem}, but the FEM and the interpolated temperature field exist in the entire domain, including in Ω_{md}. For nodes whose supports fully or partially overlap the MD region, the evolution of the nodal temperature includes a contribution from the atomic motion, so that heat information passes smoothly from the fine scale to the coarse.

1.3.3 Augmented MD

A common way of thermostatting an MD system is by adding a drag force to each atom that is proportional to the velocity of that atom [1, 2]. We can use a similar idea to include the effects of the continuum region temperature on the MD region in our coupled simulations. The equation of motion solved for each atom is

$$m_\alpha \dot{\mathbf{v}}_\alpha = \mathbf{f}_\alpha^{\text{md}} + \mathbf{f}_\alpha^{\lambda}, \tag{1.14}$$

where the classical MD force is computed from the potential energy

$$\mathbf{f}_\alpha^{\text{md}} = -\frac{\partial U^{\text{md}}}{\partial \mathbf{x}_\alpha} \tag{1.15}$$

and the drag force $\mathbf{f}_\alpha^{\lambda}$ is given by

$$\mathbf{f}_\alpha^{\lambda} = -\frac{m_\alpha}{2} \lambda_\alpha \mathbf{v}_\alpha. \tag{1.16}$$

The parameter λ_α may be different for every atom, and we assume that it is a field that can be interpolated from a set of nodal values λ_I defined on the FEM, using the nodal shape functions:

$$\lambda_\alpha(t) = \sum_I N_{I\alpha} \lambda_I(t). \tag{1.17}$$

By enforcing conservation of total energy of the system (see Wagner *et al.* [20] for details), we can derive a matrix equation for these nodal coefficients λ_I:

$$\sum_J \left(\sum_{\alpha \in \mathcal{A}} N_{I\alpha} T_\alpha N_{J\alpha} \right) \lambda_J = \frac{2}{3k_{\text{B}}} \int_{\Gamma_{\text{md}}} N_I \mathbf{n}_{\text{md}} \cdot \kappa (\nabla T^h + \tau \nabla \dot{T}^h) \, \mathrm{d}A \tag{1.18}$$

Templeton *et al.* [21] extended this approach to allow a prescribed heat flux to be applied to the boundary of an MD system through a modification of the equation for the λ_I coefficients.

The right-hand-side integral in (1.18) is a surface integral on the interface between the MD and continuum regions. In effect, this expression relates the effect that the continuum has on the MD system (through λ_I and the atomic drag forces) to the heat flux across the surface. This relation follows naturally from our conservation of total system energy, and completes the formulation. However, the numerical computation of this surface integral is not trivial, especially if the interface does not align with element boundaries. Wagner *et al.* [20] give a technique for approximating this integral using the divergence theorem together with a projection operation.

The final form of the evolution equation for the finite-element temperature field in the coupled system is [20]:

$$\begin{aligned}\sum_{J\in\mathcal{N}}\left(\int_\Omega N_I N_J\,\mathrm{d}V\right)\dot{\theta}_J = {} & \left\langle \frac{2}{3k_B}\sum_{\alpha\in\mathcal{A}} N_{I\alpha}\mathbf{v}_\alpha\cdot\left(\mathbf{f}^{\mathrm{md}}_\alpha+\frac{1}{2}\mathbf{f}^{\lambda}_\alpha\right)\Delta V_\alpha\right\rangle \\ & + \sum_{J\in\mathcal{N}}\sum_{\alpha\in\mathcal{A}}\left(\nabla N_I\cdot\frac{\kappa}{\rho c_p}\nabla N_J\right)\Big|_\alpha \theta_J\,\Delta V_\alpha \\ & - \sum_{J\in\mathcal{N}}\left(\int_\Omega \nabla N_I\cdot\frac{\kappa}{\rho c_p}\nabla N_J\,\mathrm{d}V\right)\theta_J.\end{aligned} \tag{1.19}$$

1.4 Examples

1.4.1 One-Dimensional Heat Conduction

A simple but useful demonstration of the coupled method is the transient, nonequilibrium heat flux through a quasi-one-dimensional domain [20]. Figure 1.2 shows the computational domain. The MD system represents solid argon, with $m_\alpha = 39.948$ amu and lattice constant $\ell = 5.406$ Å. Interatomic forces are computed from a Lennard-Jones potential with parameters $\varepsilon/k_{\mathrm{B}} = 119.8$ K and $\sigma = 3.405$ Å. A continuum thermal conductivity of $\kappa = 0.5$ W/(m K) was assumed in the finite-element region [22]. The computational domain comprises an MD region of size $(20 \times 8 \times 8)\ell$, centered in an overlapping finite-element domain of size $(48 \times 8 \times 8)\ell$. The entire domain was discretized using finite elements; Figure 1.2 shows a mesh size of $h = 4\ell$, giving 48 elements in the mesh.

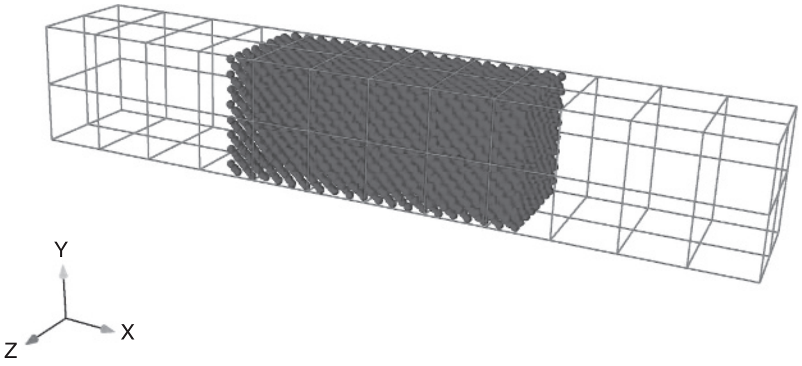

Figure 1.2 One-dimensional heat conduction: mesh and atomic positions for $h = 4\ell$

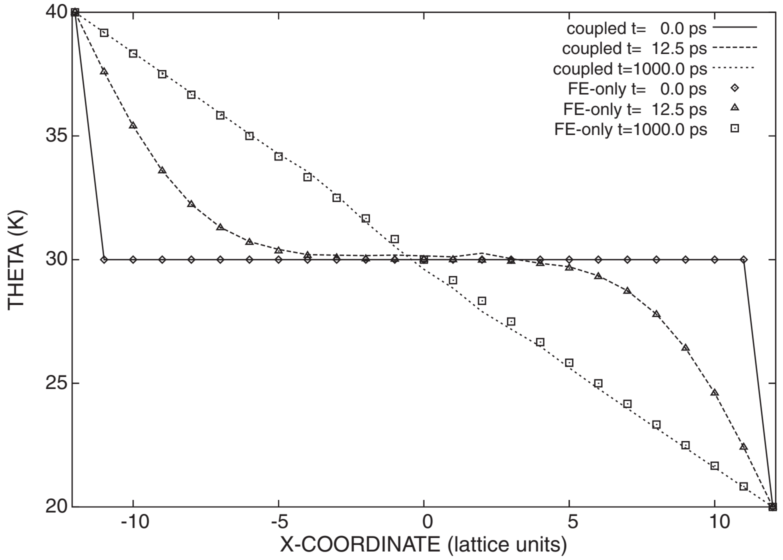

Figure 1.3 Temperature profiles for $h = 2\ell$ and $\tau = 25$ ps at $t = 0.0, 12.5, 1000.0$ ps

Periodic boundary conditions are imposed on the lateral ($\pm y$ and $\pm z$) faces of the rectangular domain. The temperature of the entire system was initially brought to 30 K via rescaling and, immediately following the thermalization stage, the end temperatures were changed to 40 K and 20 K for the left ($-x$) and right ($+x$) ends, respectively. The longitudinal temperature traces, Figure 1.3, of this essentially one-dimensional problem show good agreement with the corresponding solution of the classical heat conduction equation. There is no discernible effect in this plot of the MD–finite-element interface on the temperature solution.

1.4.2 Thermal Response of a Composite System

An extension of the coupled atomistic-to-continuum heat transfer method by Templeton *et al.* [21] allows the application of fixed temperature and heat flux boundary conditions to be specified on the continuum-scale temperature field and transmitted to the embedded MD system, even when the MD domain fills the entire continuum mesh. In this case, the goal of the coupling is not to partition the domain, but to allow the application of constraints in a straightforward way to the simulation of a nanoscale device, equivalent to the ease with which boundary conditions are applied in a typical finite-element simulation. An example is demonstrated using the domain pictured in Figure 1.4. Here, a device is represented by a block of atoms, an FCC lattice with approximate lateral dimensions of 100 nm and thickness of 25 nm. The interatomic forces for this material are assumed to be well-represented by a Lennard-Jones potential. Coating this block is a single layer of graphene-structured material, with parameters chosen to give high thermal conductivity compared with the Lennard-Jones material. An adaptive intermolecular reactive bond-order formulation [23, 24] is used to model the interactions of the graphene-structured material. Cross-interactions between the two materials are modeled with a separate set of Lennard-Jones forces. Details of parameters are given in Templeton *et al.* [21].

The MD system is overlaid with a 5 × 5 × 4 FEM, allowing the application of spatially varying boundary conditions through the finite-element temperature field. After initializing the system at 300 K, a fixed boundary temperature is applied that varies linearly in the x direction, and is also ramped linearly

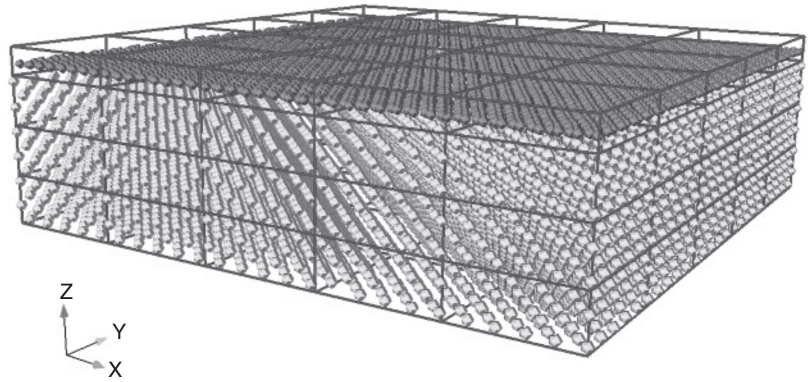

Figure 1.4 Schematic of the composite system example problem. Lennard-Jones atoms are colored light gray and graphene-structured atoms are colored dark gray. The FEM is overlaid

in time over 0.1 ns; at the final time, the $+x$ surface has a fixed temperature of 400 K, while the $-x$ surface remains at 300 K. After the device reaches an equilibrium (but spatially varying) temperature, a spatially varying heat flux with a Gaussian profile is applied on the bottom $(-z)$ face of the device, leading to further heat-up. This applied flux represents the intensity profile from laser heating of a nano-device. Figure 1.5 shows the continuum-scale temperature of top and bottom faces of the Lennard-Jones block, and of the graphene-structured layer, after 0.3 ns. An asymmetric temperature profile results in the slab from the linearly varying boundary condition. The graphene-structured layer is heated, but because of its high thermal conductivity the heat is well distributed through the layer. This example demonstrates how a coupled method like this might be used to simulate heat mitigation in a real nano-scale semiconductor device.

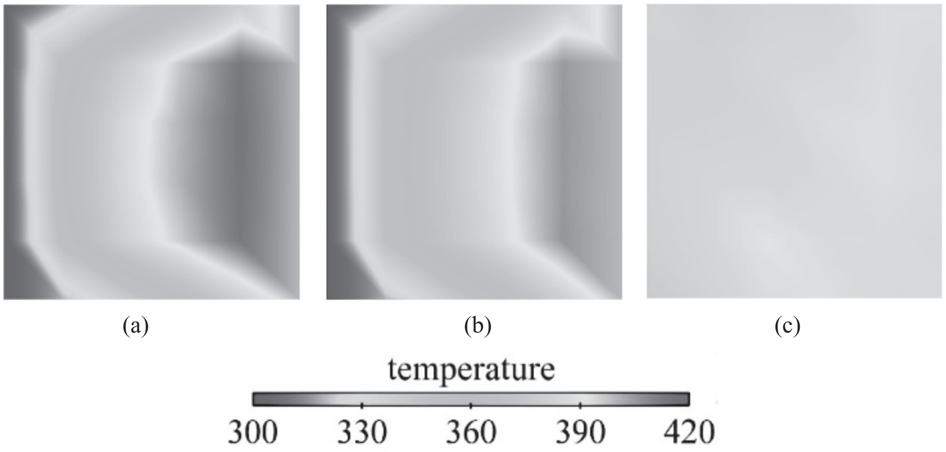
(a) (b) (c)

Figure 1.5 Time-averaged temperature profiles of the Lennard-Jones (LJ) atoms as viewed from the bottom (a) and top (b), compared with the graphene-structured layer (c). Temperatures are in kelvin

1.5 Coupled Phonon-Electron Heat Transport

As discussed in Section 1.1, the role of electrons in the transport of heat is crucial in metals and semimetals. In classical MD simulations, this electron transport is missing. On the other hand, MD represents well the transport of heat by phonons, in both the ballistic and diffusive regimes [25–27]; a method that couples the phonon and electron modes of heat transport can allow more accurate simulations of thermal behavior for a number of applications, including laser processing of materials [28–31], thermoelectric material design [32–35], heat transport in conducting nanotubes and nanowires [32, 36], and heat transport at material interfaces [37].

A well-explored method for coupling phononic and electronic heat transport is the TTM [38–42]. This model treats the internal energy residing in both sets of carriers as a continuum temperature field; energy is transferred between the two fields through an exchange term that ensures conservation of the total energy:

$$\rho_\mathrm{e} c_\mathrm{e} \dot{T}_\mathrm{e} = -\nabla \cdot \mathbf{q}_\mathrm{e} - g + S_\mathrm{e}, \tag{1.20a}$$

$$\rho_\mathrm{p} c_\mathrm{p} \dot{T}_\mathrm{p} = -\nabla \cdot \mathbf{q}_\mathrm{p} + g + S_\mathrm{p}. \tag{1.20b}$$

The temperatures T, densities ρ, heat capacities c, heat fluxes $\mathbf{q}$, and source terms S are subscripted with “e” or “p” to denote the electron or phonon quantities. The heat fluxes are typically modeled as functions of their respective temperatures and temperature gradients (e.g., $\mathbf{q}_\mathrm{p} = -\kappa_\mathrm{p} \nabla T_\mathrm{p}$ in the Fourier model). The energy exchange g is the rate of heat transferred from the electrons to the phonons, and is usually taken as a function of the temperature difference between the two sets of carriers, $g = g(T_\mathrm{e} - T_\mathrm{p})$. In this model, both temperature fields exist everywhere in the solution domain.

Replacing the continuum representation of the phonon temperature (Equation (1.20b)) with an MD system requires a procedure for injecting energy into the phonons that is equal to the energy lost by the electrons, so that energy conservation is maintained. This energy exchange is still desired to be a function of the difference between the phonon and electron energy, where now the phonon energy must be computed through some spatial–temporal averaging on the MD system, as in earlier sections in this chapter. Jones *et al.* [13] developed a method that ensures this energy conservation, and at the same time allows a domain partitioning such that a finite-element representation of the phonon temperature can be used where a continuum representation is sufficient, and MD can be used locally in regions where it is not.

The geometry partitioning considered is like that represented in Figure 1.1, with an MD system embedded locally in an overlaying FEM. In the TTM case, both the phonon and electron temperatures are represented as interpolated fields everywhere on the FEM. As in Section 1.3, the total energy is partitioned between the MD and FEM parts:

$$E^\mathrm{tot} = E^\mathrm{md} + E^\mathrm{fem}. \tag{1.21}$$

However, now the continuum-scale energy includes both the phonon energy in the FEM region Ω_fem and the electron energy in the entire domain Ω:

$$E^\mathrm{fem} = \int_{\Omega_\mathrm{fem}} \rho_\mathrm{p} c_\mathrm{p} T_\mathrm{p} \,\mathrm{d}V + \int_{\Omega} \rho_\mathrm{e} c_\mathrm{e} T_\mathrm{e} \,\mathrm{d}V. \tag{1.22}$$

The MD energy is again the sum of the potential and kinetic energies of the atoms:

$$E^\mathrm{md} = U^\mathrm{md} + \frac{1}{2} \sum_{\alpha} m_\alpha |\mathbf{v}_\alpha|^2. \tag{1.23}$$

Note that Jones *et al.* [13] do not consider time filtering. As in previous sections (cf. Equation (1.14)), an augmented molecular dynamics force is used, where the added drag force is again

$$\mathbf{f}_\alpha^\lambda = -\frac{m_\alpha}{2}\mathbf{v}_\alpha \sum_I N_{I\alpha}\lambda_I. \tag{1.24}$$

An expression for the nodal coefficients λ_I that define the drag force on the atoms can be derived through an energy conservation equation. For simplicity, let us assume that a heat flux $\bar{q}$ in the direction of the outward normal is defined everywhere on the outer boundary Γ in Figure 1.1. The change in the total energy is determined by this boundary heat flux and the source terms S_p and S_e:

$$\dot{E}^{tot} = \int_\Omega (S_\mathrm{p} + S_\mathrm{e})\,\mathrm{d}V - \int_\Gamma \bar{q}\,\mathrm{d}A. \tag{1.25}$$

Taking the time derivatives of (1.22) and (1.23) and substituting into (1.25) gives

$$\begin{aligned}\int_\Omega (S_\mathrm{p} + S_\mathrm{e})\,\mathrm{d}V - \int_\Gamma \bar{q}\,\mathrm{d}A = &-\frac{1}{2}\sum_\alpha m_\alpha|\mathbf{v}_\alpha|^2 \sum_J N_{J\alpha}\lambda_J \\ &+ \int_{\Omega_\mathrm{fem}} (-\nabla\cdot\mathbf{q}_\mathrm{p} + g + S_\mathrm{p})\,\mathrm{d}V \\ &+ \int_\Omega (-\nabla\cdot\mathbf{q}_\mathrm{e} - g + S_\mathrm{e})\,\mathrm{d}V.\end{aligned} \tag{1.26}$$

In arriving at this expression we have assumed that Equation (1.20a) applies in Ω and applied in Ω_fem (i.e., outside the MD system); we have also used (1.14) and (1.24) to rewrite the rate of change of the MD energy. Using the divergence theorem on the heat flux integrals, noting that the boundary heat flux $\bar{q}$ on Γ is composed of phonon and electron parts, and canceling some integrals gives a global energy conservation expression of the form

$$\frac{3k_\mathrm{B}}{2}\sum_\alpha T_\alpha \sum_J N_{J\alpha}\lambda_J = -\int_{\Omega_\mathrm{md}} (S_\mathrm{p} + g)\,\mathrm{d}V - \int_{\Gamma_\mathrm{md}} \mathbf{n}_\mathrm{md}\cdot\mathbf{q}_\mathrm{p}\,\mathrm{d}A. \tag{1.27}$$

The definition of the atomic temperature from (1.2) has been used to simplify this expression. The left-hand side of this expression is related to the energy removed from the MD system by the augmented force term, through the coefficients λ_J. The right-hand side represents the change in the phonon energy in Ω_md due to source and electron transfer terms, as well as heat flux across the boundary at the continuum interface. The minus sign on the right-hand side corresponds to the fact that positive values of the λ_J represent a drag force that removes energy from the MD system.

In order to write an expression that can be solved for the λ_J coefficients, we can take this global energy balance and localize it through the use of finite-element shape functions N_I:

$$\frac{3k_\mathrm{B}}{2}\sum_J\sum_\alpha N_{I\alpha}T_\alpha N_{J\alpha}\lambda_J = -\int_{\Omega_\mathrm{md}} N_I(S_\mathrm{p} + g)\,\mathrm{d}V - \int_{\Gamma_\mathrm{md}} N_I\mathbf{n}_\mathrm{md}\cdot\mathbf{q}_\mathrm{p}\,\mathrm{d}A. \tag{1.28}$$

Satisfaction of (1.28) implies satisfaction of (1.27), which can be verified by summing (1.28) over all nodes I and noting that the finite-element shape functions are a partition of unity ($\sum_I N_I = 1$). However, (1.28) is not the only localized form that guarantees global energy conservation, and alternatives are possible that result in modified expressions.

Equation (1.28) defines a matrix equation for the nodal coefficients λ_J in terms of known quantities that are either given or computable from the continuum electron and phonon temperature fields. Comparison with the similar Equation (1.18) derived for the case without electrons shows that the expressions are equivalent in the absence of source and electron transfer terms, if a Fourier law is used for the phonon heat transfer at the boundary and if time filtering is ignored ($\tau = 0$).

Jones *et al.* [13] also derived governing equations for the finite-element fields representing the electron and phonon temperatures. These fields are parameters by nodal coefficients θ_{eJ} and θ_{pJ}, respectively, and satisfy the following weak forms of the energy equation:

$$\sum_J \left(\int_\Omega N_I \rho_e c_e N_J \, dV \right) (\dot{\theta}_e)_J = \int_\Omega [\nabla N_I \cdot \mathbf{q}_e + N_I (S_e - g)] \, dV - \int_\Gamma N_I \bar{q}_e \, dA, \tag{1.29a}$$

$$\begin{aligned} \sum_J \left(\int_\Omega N_I \rho_p c_p N_J \, dV \right) (\dot{\theta}_p)_J &= 2 \sum_\alpha N_{I\alpha} \mathbf{v}_\alpha \cdot \left(\mathbf{f}_\alpha^{\mathrm{md}} + \mathbf{f}_\alpha^\lambda \right) \\ &+ \int_{\Omega_{\mathrm{fem}}} [\nabla N_I \cdot \mathbf{q}_p + N_I (S + g)] \, dV - \int_\Gamma N_I \bar{q}_p \, dA. \end{aligned} \tag{1.29b}$$

In these equations, it is assumed that the prescribed heat flux $\bar{q}$ on the boundary Γ can be decomposed into phonon ($\bar{q}_p$) and electron parts ($\bar{q}_e$). These two equations, together with (1.14) for each atom and (1.28) for the nodal λ coefficients, completes the set of equations to be solved for the coupled MD–FEM, TTM system.

1.6 Examples: Phonon–Electron Coupling

1.6.1 Equilibration of Electron/Phonon Energies

A simple verification of the method for domain-partitioned MD–FEM with a TTM is obtained through simulation of a block of material in which the electrons have an initial temperature that is spatially varying and higher than the initial phonon temperature. Over time we expect that the two sets of carriers should equilibrate to a constant, common temperature. The test domain is shown in Figure 1.6. A square film of material 24 unit cells on each side and six unit cells deep is represented by a 12 × 12 × 1 FEM; periodic boundary conditions are used in the out-of-plane direction. The central 12 × 12 unit cells of the domain are represented with atoms whose interatomic force is computed from a Lennard-Jones potential. In Figure 1.6, the dark atoms are "ghost" atoms used to constrain the inner MD system and provide a full complement of neighbors for all of the atoms. The exchange energy g is assumed to be a linear function of the temperature difference between electrons and phonons: $g = g_{e\text{–}p}(T_e - T_p)$. Geometry, interatomic potential, and material parameters are taken from Jones *et al.* [13].

The initial temperature of the phonons is 20 K, and in the simulation an initial equilibration phase is used to thermostat the MD system at this temperature. The initial electron temperature is a radially varying function with a Gaussian profile, $T_e = 20[3\,e^{(r/25)^2} + 5]$ (in degrees kelvin), where $r = (x^2 + y^2)^{1/2}$ is the distance from the center of the domain in the x–y plane. After initialization, the system is run with no other source terms and with adiabatic ($\bar{q}_e = \bar{q}_p = 0$) boundary conditions. In Figure 1.6, the FEM is colored by the initial electron temperature, while the atoms are colored by the instantaneous values of the atomic temperature T_α at time $t = 0$.

Figure 1.7a shows a time sequence of temperature profiles measured along the x-axis. A combination of diffusion and phonon-electron exchange drive the temperatures to a spatially constant common value. Spatial fluctuations in the phonon temperature are visible in the central region because of the stochastic nature of the MD system. In Figure 1.7b, the conservation of total energy is demonstrated; the energy of the electrons decreases while that of the phonons and MD system increase, such that the total remains constant in this adiabatic system.

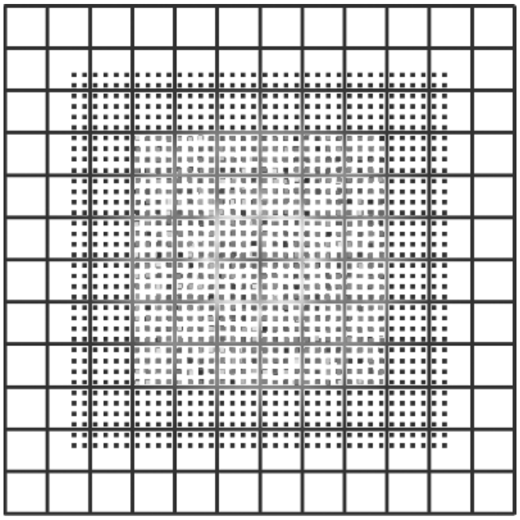

Figure 1.6 Configuration of the MD lattice (colored by the atomic temperature T_α) embedded in a finite-element grid (colored by the electron temperature). Note the five layers of ghosts (dark color) are fixed and, therefore, have zero kinetic temperature

1.6.2 Laser Heating of a Carbon Nanotube

Another example application is the heating of a carbon nanotube [13]. A metallic (8, 8) armchair nanotube, with length 12.6 nm, is suspended with its ends embedded in solid graphite (Figure 1.8). The nanotube is modeled using a Tersoff potential for the interatomic forces [43], while the graphite is modeled as a continuum with the same thermal properties as the nanotube. For a nanotube, the phonon

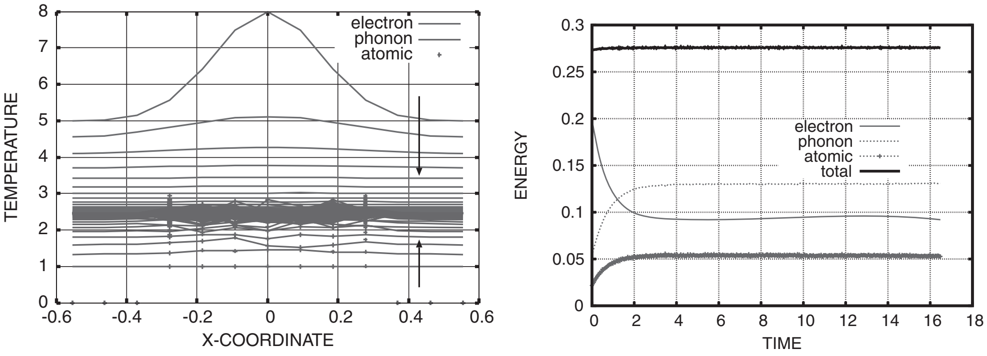

(a) (b)

Figure 1.7 (a) Sequence of temperature profiles through a cross-section aligned with the x-axis. The arrows indicate the progression of profiles with time. (b) Evolution of energy. The atomic thermal energy is calculated for the lattice, phonon energy is calculated in Ω_{fem}, and the electron energy is integrated over the full domain Ω

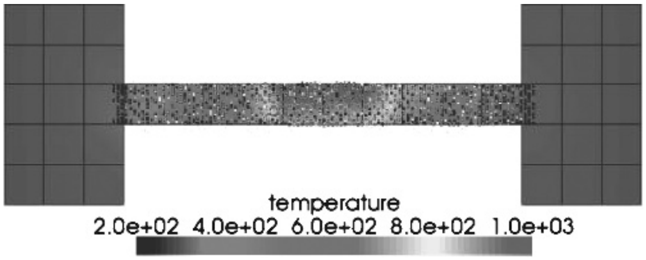

Figure 1.8 Metallic carbon nanotube embedded in an FEM showing phonon temperature near the beginning of the heating phase, $t = 10$ ps

electron exchange is highly nonlinear in temperature [44], $g = h(T_\mathrm{e} - T_\mathrm{p})^5$ with $h = 3.7 \times 10^4$ W/m^{3}K^5. Experiments [25] demonstrate mixed ballistic and diffusive modes of heat transport due to phonon transport in carbon nanotubes, and the MD representation is able to model both of these modes.

The ends of the graphene regions are held fixed at $T_\mathrm{e} = T_\mathrm{p} = 300$ K. Laser heating of the nanotube is modeled with a source term on the electron energy that is spatially varying:

$$S_\mathrm{e} = (1.6 \times 10^{-12}\ \mathrm{W/m^3})\ \exp\left(-\frac{x^2 + y^2}{0.01}\right), \tag{1.30}$$

where distances are measured in nanometers. This source term is applied for a time of 50 ps and the system is then allowed to relax.

Figure 1.9 shows sequences of temperature profiles over time for both the phonon and electron temperatures. The electrons, which are heated directly, show a very localized heating, while the indirectly heated phonons have a more diffuse temperature profile.

Figure 1.10 shows the average temperatures of the nanotube and the graphene reservoirs over time. The large oscillations in the nanotube temperature correspond to the excitation of a fundamental mode resonance in the tube, as can be seen in a plot of the displaced atoms and mesh in Figure 1.11.

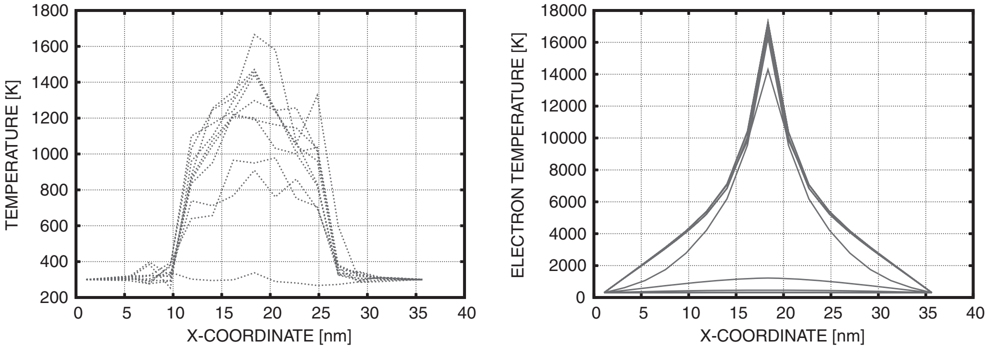

(a) (b)

Figure 1.9 Sequence of (a) temperature and (b) electron temperature profiles along the axis of the carbon nanotube. Note that the two plots show different temperature ranges

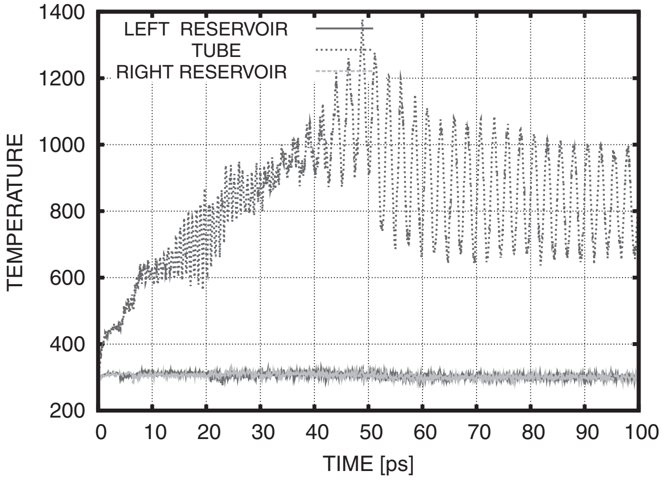

Figure 1.10 Evolution of average temperatures of the two explicitly modeled reservoirs and the carbon nanotube

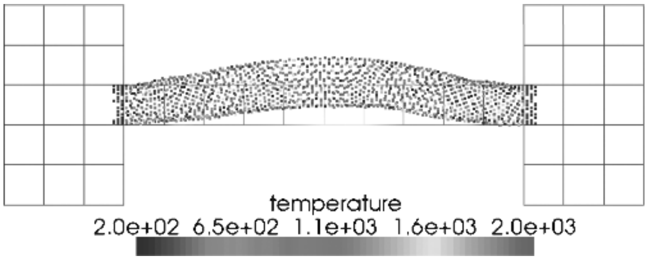

Figure 1.11 Fundamental mode excited by focused irradiation. The atoms and the mesh are both colored by the phonon temperature

1.7 Discussion

The methods and demonstrations in this chapter represent steps toward the ability to simulate heat transfer in nanoscale systems, including non-continuum effects, with the same ease with which finite-element models can today be used to define and solve macroscale heat transfer problems. Through the coupled atomistic-to-continuum approach, we are able to apply spatially varying boundary and initial conditions on temperature, as well as spatially and temporally varying heat fluxes, to MD systems. At the same time, we can choose to use MD only in isolated regions of the domain, improving computational efficiency. Finally, we can use the coupling to a continuum field to capture effects, such as electronic heat transfer, that are otherwise missed by classical MD simulations.

It should be pointed out that many of the assumptions made in the continuum models presented in this chapter are easy to relax in the methods presented. For example, although we have assumed that a Fourier heat law describes the continuum region in Section 1.3.2, it is straightforward to replace this with the Maxwell–Cattaneo–Vernotte model typically employed to represent the finite speed of propagation of heat waves [45, 46]; the derivation of the coupled system proceeds in a similar way.

Likewise, a drift-diffusion model [47] can be used for the electron energy propagation rather than the simpler Fourier-diffusion form used in Section 1.5; the drift-diffusion model is explored in this context by Jones *et al.* [48].

An efficient, portable implementation of any new computational method is key to its future development and usefulness. To this end, many of the interscale coupling operations used in the work presented in this chapter have been implemented as an optional package available with the popular LAMMPS MD code [49], available for download at (http://lammps.sandia.gov). The USER-ATC package within LAMMPS includes FEM definitions, projection operators, interpolation functions, coupling thermostats, time integrators, and post-processors that enable the simulations presented in this chapter.

Acknowledgments

Sandia National Laboratories is a multi-program laboratory managed and operated by Sandia Corporation, a wholly owned subsidiary of Lockheed Martin Corporation, for the US Department of Energy's National Nuclear Security Administration under contract DE-AC04-94AL85000.

References

[1] Berendsen, H., Postma, J., Vangunsteren, W. *et al.* (1984) Molecular-dynamics with coupling to an external bath. *Journal of Chemical Physics*, **81** (8), 3684–3690.

[2] Hoover, W. (1985) Canonical dynamics – equilibrium phase-space distributions. *Physical Review A*, **31** (3), 1695–1697.

[3] Curtin, W. and Miller, R. (2003) Atomistic/continuum coupling in computational materials science. *Modelling and Simulation in Materials Science and Engineering*, **11** (3), R33–R68.

[4] Park, H. and Liu, W. (2004) An introduction and tutorial on multiple-scale analysis in solids. *Computer Methods in Applied Mechanics and Engineering*, **193** (17–20), 1733–1772.

[5] Abraham, F., Broughton, J., Bernstein, N., and Kaxiras, E. (1998) Spanning the length scales in dynamic simulation. *Computers in Physics*, **12** (6), 538–546.

[6] Knap, J. and Ortiz, M. (2001) An analysis of the quasicontinuum method. *Journal of the Mechanics and Physics of Solids*, **49** (9), 1899–1923.

[7] Miller, R. and Tadmor, E. (2009) A unified framework and performance benchmark of fourteen multiscale atomistic/continuum coupling method. *Modelling and Simulation in Materials Science and Engineering*, **17** (5), 053001.

[8] Cai, W., de Koning, M., Bulatov, V., and Yip, S. (2000) Minimizing boundary reflections in coupled-domain simulations. *Physical Review Letters*, **85** (15), 3213–3216.

[9] Wagner, G. and Liu, W. (2003) Coupling of atomistic and continuum simulations using a bridging scale decomposition. *Journal of Computational Physics*, **190** (1), 249–274.

[10] To, A. and Li, S. (2005) Perfectly matched multiscale simulations. *Phys Rev B*, **72** (3), 035414.

[11] Ivanov, D. and Zhigilei, L. (2003) Combined atomistic-continuum modeling of short-pulse laser melting and disintegration of metal films. *Physical Review B*, **68** (6), 064114.

[12] Xu, X., Cheng, C., and Chowdhury, I. (204) Molecular dynamics study of phase change mechanisms during femtosecond laser ablation. *ASME Journal of Heat Transfer*, **126** (5), 727–734.

[13] Jones, R., Templeton, J., Wagner, G. *et al.* (2010) Electron transport enhanced molecular dynamics for metals and semi-metals. *International Journal for Numerical Methods in Engineering*, **83** (8–9), 940–967.

[14] Qian, D., Wagner, G., and Liu, W. (2004) A multiscale projection method for the analysis of carbon nanotubes. *Computer Methods in Applied Mechanics and Engineering*, **193** (17-20), 1603–1632.

[15] Liu, W., Park, H., Qian, D. *et al.* (2006) Bridging scale methods for nanomechanics and materials. *Computer Methods in Applied Mechanics and Engineering*, **195** (13–16), 1407–1421.

[16] Liu, W., Uras, R., and Chen, Y. (1997) Enrichment of the finite element method with the reproducing kernel particle method. *Journal of Applied Mechanics, ASME*, **64** (4), 861–870.

[17] Uras, R., Chang, C., Chen, Y., and Liu, W. (1997) Multiresolution reproducing kernel particle methods in acoustics. *Journal of Computational Acoustics*, **5** (1), 71–94.

[18] Wagner, G. and Liu, W. (2001) Hierarchical enrichment for bridging scales and mesh-free boundary conditions. *International Journal for Numerical Methods in Engineering*, **50** (3), 507–524.

[19] Weiner, J. (2002) *Statistical Mechanics of Elasticity*, 2nd edition, Dover, Mineola, NY.

[20] Wagner, G., Jones, R., Templeton, J., and Parks, M. (2008) An atomistic-to-continuum coupling method for heat transfer in solids. *Computer Methods in Applied Mechanics and Engineering*, **197** (41–42), 3351–3365.

[21] Templeton, J., Jones, R., and Wagner, G. (2010) Application of a field-based method to spatially varying thermal transport problems in molecular dynamics. *Modelling and Simulation in Materials Science and Engineering*, **18** (8), 085007.

[22] Tretiakov, K. and Scandolo, S. (2004) Thermal conductivity of solid argon from molecular dynamics simulations. *Journal of Chemical Physics*, **120** (8), 3765–3769.

[23] Stuart, S., Tutein, A., and Harrison, J. (2000) A reactive potential for hydrocarbons with intermolecular interactions. *Journal of Chemical Physics*, **112** (14), 6472–6486.

[24] Brenner, D., Shenderova, O., Harrison, J. *et al.* (2002) A second-generation reactive empirical bond order (REBO) potential energy expression for hydrocarbons. *Journal of Physics: Condensed Matter*, **14** (4), 783–802.

[25] Wang, J. and Wang, J. (2006) Carbon nanotube thermal transport: ballistic to diffusive. *Applied Physics Letters*, **88** (11), 111909.

[26] Chen, R., Hochbaum, A., Murphy, P. *et al.* (2008) Thermal conductance of thin silicon nanowires. *Physical Review Letters*, **101** (10), 105501.

[27] Chang, C., Okawa, D., Garcia, H. *et al.* (2008) Breakdown of Fourier's law in nanotube thermal conductors. *Physical Review Letters*, **101** (7), 075903.

[28] Chrisey, D. and Hubler, G. (1994) *Pulsed Laser Deposition of Thin Films*, Wiley Interscience, New York, NY.

[29] Baerle, D. (2000) *Laser Processing and Chemistry*, Springer, Berlin.

[30] Sundaram, S. and Mazur, E. (2002) Inducing and probing non-thermal transitions in semiconductors using femtosecond laser pulses. *Nature Materials*, **1** (4), 217–224.

[31] Wang, Y., Xu, X., and Zheng, L. (2008) Molecular dynamics simulation of ultrafast laser ablation of fused silica film. *Applied Physics A: Materials Science & Processing*, **92** (4), 849–852.

[32] Kim, P., Shi, L., Majumdar, A., and McEuen, P. (2001) Thermal transport measurements of individual multiwalled nanotubes. *Physical Review Letters*, **87** (21), 215502.

[33] Yang, B., Liu, W., Liu, J. *et al.* (2002) Measurements of anisotropic thermoelectric properties in superlattices. *Applied Physics Letters*, **81** (19), 3588–3590.

[34] Li, D., Wu, Y., Fan, R. *et al.* (2003) Thermal conductivity of Si/SiGe superlattice nanowires. *Applied Physics Letters*, **83** (15), 3186–3188.

[35] Snyder, G. and Toberer, E. (2008) Complex thermoelectric materials. *Nature Materials*, **7** (2), 105–114.

[36] Ou, M., Yang, T., Harutyunyan, S. *et al.* (2008) Electrical and thermal transport in single nickel nanowire. *Applied Physics Letters*, **92** (6), 063101.

[37] Majumdar, A. and Reddy, P. (2004) Role of electron–phonon coupling in thermal conductance of metal–nonmetal interfaces. *Applied Physics Letters*, **84** (23), 4768–4770.

[38] Kaganov, M., Lifshits, I., and Tanatarov, L. (1956) Relaxation between electrons and the crystal lattice. *Zhurnal Eksperimental'noi i Teoreticheskoi Fiziki*, **31** (2(8)), 232–237.

[39] Anisimov, S., Kapeliov, B., and Perelman, T. (1998) Emission of electrons from the surface of metals induced by ultrashort laser pulses. *Zhurnal Eksperimental'noi i Teoreticheskoi Fiziki*, **66** (2), 776–781.

[40] Qiu, T. and Tien, C. (1993) Heat transfer mechanisms during short-pulse laser heating of metals. *Journal of Heat Transfer*, **115** (4), 835–841.

[41] Melikyan, A., Minassian, H., Guerra, III, A., and Wu, W. (1999) On the theory of relaxation of electrons excited by femtosecond laser pulses in thin metallic films. *Applied Physics B: Lasers and Optics*, **68** (3), 411–414.

[42] Jiang, L. and Tsai, H. (2005) Improved two-temperature model and its application in ultrashort laser heating of metal films. *Journal of Heat Transfer*, **127** (10), 1167–1173.

[43] Tersoff, J. (1988) Empirical interatomic potential for carbon, with applications to amorphous carbon. *Physical Review Letters*, **61** (25), 2879–2882.

[44] Hertel, T., Fasel, R., and Moos, G. (2002) Charge-carrier dynamics in single-wall carbon nanotube bundles: a time-domain study. *Applied Physics A: Materials Science & Processing*, **75** (4), 449–465.
[45] Joseph, D. and Preziosi, L. (1989) Heat waves. *Reviews of Modern Physics*, **61** (1), 41–73.
[46] Ho, J.R., Twu, C.J., and Hwang, C.C. (2001) Molecular-dynamics simulation of thermoelastic waves in a solid induced by a strong impulse energy. *Physical Review B*, **64** (1), 014302.
[47] Chen, G. (2005) *Nanoscale Energy Transport and Conversion*, Oxford University Press, Oxford.
[48] Jones, R., Templeton, J., Modine, N. *et al.* (2010) Molecular dynamics enhanced with electron transport, Technical Report SAND2010-6164, Sandia National Laboratories.
[49] Plimpton, S. (1995) Fast parallel algorithms for short-range molecular-dynamics. *Journal of Computational Physics*, **117** (1), 1–19.